Supporting Information

Origin of Magnetism in Hydrothermally Aged 2-line Ferrihydrite Suspensions

Liang Cao,[†,‡] Zhao-Xia Jiang,[§] Yong-Hua Du,[‖] Xin-Mao Yin,[⊥,#] Shi-Bo Xi,[‖] Wen Wen,[†]

Andrew P. Roberts,[▽] Andrew T. S. Wee,[⊥] Yi-Min Xiong,[‡] Qing-Song Liu,*[,○,♦] Xing-Yu Gao*[,†]

† Shanghai Institute of Applied Physics, Chinese Academy of Sciences, P. O. Box 800–204, Shanghai, 201800, P. R. China

‡ High Magnetic Field Laboratory, Chinese Academy of Sciences, 350 Shushanhu Road, Hefei, Anhui, 230031, P. R. China

§ State Key Laboratory of Lithospheric Evolution, Institute of Geology and Geophysics, Chinese Academy of Sciences, 19 Beitucheng Western Road, Beijing, 100029, P. R. China

|| Institute of Chemical and Engineering Sciences, A*STAR (Agency for Science, Technology and Research), 1 Pesek Road, Jurong Island, 627833, Singapore

⊥ Department of Physics, National University of Singapore, 2 Science Drive 3, 117542, Singapore

SZU-NUS Collaborative Innovation Center for Optoelectronic Science & Technology, Key Laboratory of Optoelectronic Devices and Systems of Ministry of Education and Guangdong Province, College of Optoelectronic Engineering, Shenzhen University, Shenzhen, 518060, P. R. China

∇ Research School of Earth Sciences, The Australian National University, 142 Mills Road, Canberra, ACT 2601, Australia

○ Department of Marine Science and Engineering, Southern University of Science and Technology of China, Shenzhen, 518055, P. R. China

♦ Laboratory for Marine Geology, Qingdao National Oceanography Laboratory for Science and Technology, Qingdao, 266071, P. R. China

* Corresponding Authors:

qsliu@sustc.edu.cn. Phone: (86)-10-82998365. (Q.-S. L.);

gaoxingyu@sinap.ac.cn. Phone: (86)-21-3393-3199. (X.-Y. G.).

Number of pages: 11

Number of Figures: 7

Number of Tables: 1

XMCD spectrum. An XMCD spectrum for 6-line ferrihydrite was measured at room temperature, which is above the blocking temperature of 6-line ferrihydrite. It is, therefore, expected that the signal will be close to the noise level of the synchrotron detectors.

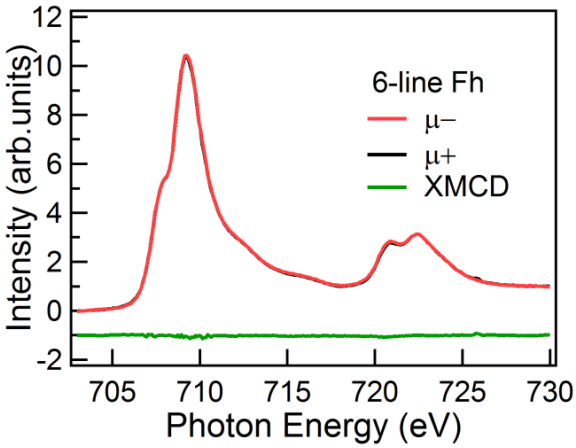

Figure S1. XMCD spectrum of 6-line ferrihydrite (Fh) measured at room temperature.

XMCD spectra of hydrothermally aged ferrihydrite are fitted by a linear combination of γ-Fe_2O_3 and Fe_3O_4 reference spectra (**Figure S2**). The existence of Fe_3O_4 during hydrothermal aging can be ruled out because the fitted spectra have a contribution only from the γ-Fe_2O_3 spectrum with an uncertainty no larger than 3%, which supports the conclusions drawn from Fe *L*-edge XAS and *K*-edge XANES curve-fitting results. The fitting curve for FAl0-08 almost perfectly reproduces the experimental data. However, XMCD spectra for 6 h and 10 h aged ferrihydrite have stronger positive tetrahedral Fe^{3+} ($T_d(Fe^{3+})$) than that in the fitted spectra, which suggests that the $T_d(Fe^{3+})$ could be stronger in those samples than in γ-Fe_2O_3 possibly due to a complicated spin arrangement among different sites in the ferrihydrite core and the γ-Fe_2O_3 shell structures. The XMCD spectra calculated as the intensity difference of XAS spectra naturally have a much larger noise to signal ratio, which inevitably also leads to a larger fitting uncertainty.

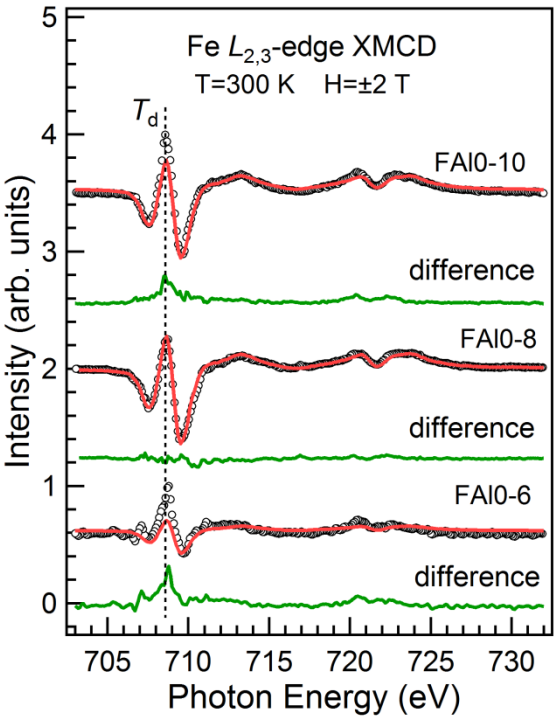

Figure S2. Fe $L_{2,3}$-edge XMCD spectra for the three studied 2-line ferrihydrite samples with different hydrothermal aging times. The red curves represent best fits by linear combination of γ-Fe_2O_3 and Fe_3O_4 reference spectra. Difference spectra between fitted and experimental data are shown in green.

Crystal Structure. Synchrotron-based X-ray diffraction (XRD) measurements were made at the BL14B1 beamline of the Shanghai Synchrotron Radiation Facility (SSRF) with a wavelength of 0.6887 Å.[1] Measurements were made in spinning capillary mode, with samples loaded into a 0.5-mm glass capillary. A Mythen 1 K linear detector, which is mounted on the diffraction arm ~76 cm away from the sample, was employed for data acquisition. The typical angular resolution is ~ 0.0037°/channel (1280 channels cover a 2θ range of 4.8º). Acquisition time for one scan is ~1 minute. The data were analyzed using the CMPR program1 for background subtraction (empty capillary).

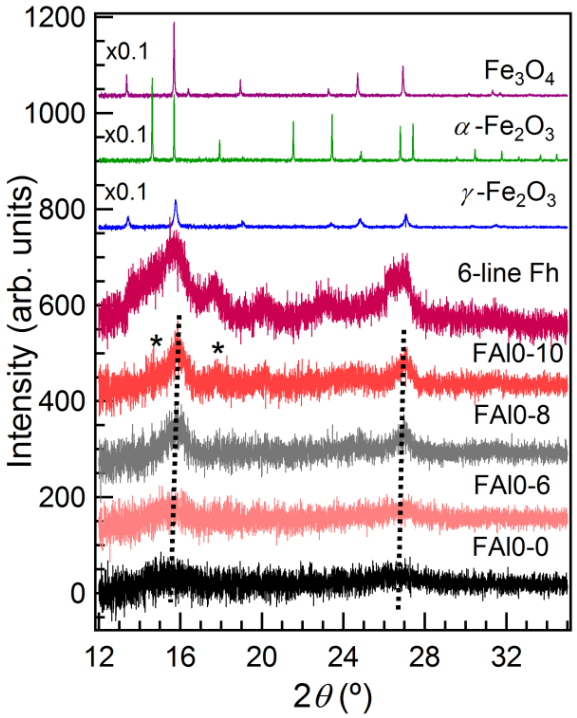

Figure S3. X-ray diffraction patterns for the four studied 2-line ferrihydrite samples (wavelength of 0.6887 Å). Standard diffraction patterns for 6-line ferrihydrite, α-Fe_2O_3, γ-Fe_2O_3 and Fe_3O_4 are also shown.

The crystal structure of the reference samples and the studied 2-line ferrihydrite samples was further characterized by XRD (**Figure S3)**. Two prominent diffraction peaks for samples aged for 10 h are located at ~15.86° and ~26.95°, respectively. The corresponding *d* spacings are 2.50 Å and 1.48 Å, respectively. The diffraction intensity increases with hydrothermal aging time, which demonstrates that crystallinity is enhanced during hydrothermal aging. All peaks shift to higher 2θ angles during hydrothermal aging, which suggests a systematic structural change in the samples. To explain this behavior, the diffraction pattern for the sample after 10 hours of aging at 450 K is compared with diffraction patterns for α-Fe_2O_3, γ-Fe_2O_3, Fe_3O_4 and 6-line ferrihydrite standards. Although all of the standards have diffraction peaks at around 15.86° and 26.95°, the

two peaks for Fe_3O_4 occur at slightly smaller angles than for γ-Fe_2O_3 and for the sample after 10 hours of aging at 450 K. Moreover, based on diffraction peaks at ~15.86° and ~26.95°, the calculated lattice parameter is not consistent with that of a cubic unit cell for Fe_3O_4. For a tetragonal structure, lattice parameters of $a = b = 8.49$ Å and $c = 24.70$ Å are obtained. Thus, Fe_3O_4 should not exist in this sample. Moreover, the weak (asterisked) peaks in **Figure S3** may originate from 6-line ferrihydrite and/or α-Fe_2O_3. The peak at ~20.09° after 10 hours of aging at 450 K is attributed to 6-line ferrihydrite. This sample should, therefore, contain both γ-Fe_2O_3 and α-Fe_2O_3, but not Fe_3O_4, which supports our XMCD and XAS results.

Local structure around Fe atoms: To understand the evolution of the local structure around Fe atoms in ferrihydrite with increasing hydrothermal aging time, *K*-edge extended X-ray absorption fine structure (EXAFS) spectra were measured for standard α-Fe_2O_3, γ-Fe_2O_3, Fe_3O_4, 6-line ferrihydrite and the four studied 2-line ferrihydrite samples (**Figure S4**(a)). Corresponding phase-shift uncorrected *K*-edge Fourier transform EXAFS spectra are shown in **Figure S4**(b). The first single coordination peak in the 1~2 Å region corresponds to the first Fe-O coordination shells in Fe atoms. The second peak corresponds to the Fe-Fe interatomic distance in second coordination shells. Peaks for α-Fe_2O_3, γ-Fe_2O_3 and Fe_3O_4 standards are located at ~2.47 Å and ~2.57 Å, respectively.

In general, EXAFS features resemble those of the (α-/γ-)Fe_2O_3 standards and are clearly different from those of the Fe_3O_4 standard, which indicates that Fe_3O_4 does not exist in these samples. The Fe-Fe coordination peak of 2-line ferrihydrite is located at ~2.57 Å, which is comparable with the value for γ-Fe_2O_3. Its position decreases gradually to lower values with hydrothermal aging time, and reaches ~2.50 Å after 10 h of aging at 450 K, which suggests a systematic structural change, such as a reduced distortion due to an ordered structure or

dehydration of the mineral surface that resulted from decreased Fe-Fe interatomic distance. It is accepted that spectra for multi-site minerals indicate an intermediate structure. Peak positions for the studied ferrihydrite samples associated with Fe-O coordination (dashed-dot line in **Figure S4**(b)) and Fe-Fe coordination (solid bars in **Figure S4**(b)) all lie between values for α-Fe_2O_3 and γ-Fe_2O_3, which indicates that the aged samples contain both γ-Fe_2O_3 and α-Fe_2O_3, but not Fe_3O_4, which supports our XMCD and XAS results.

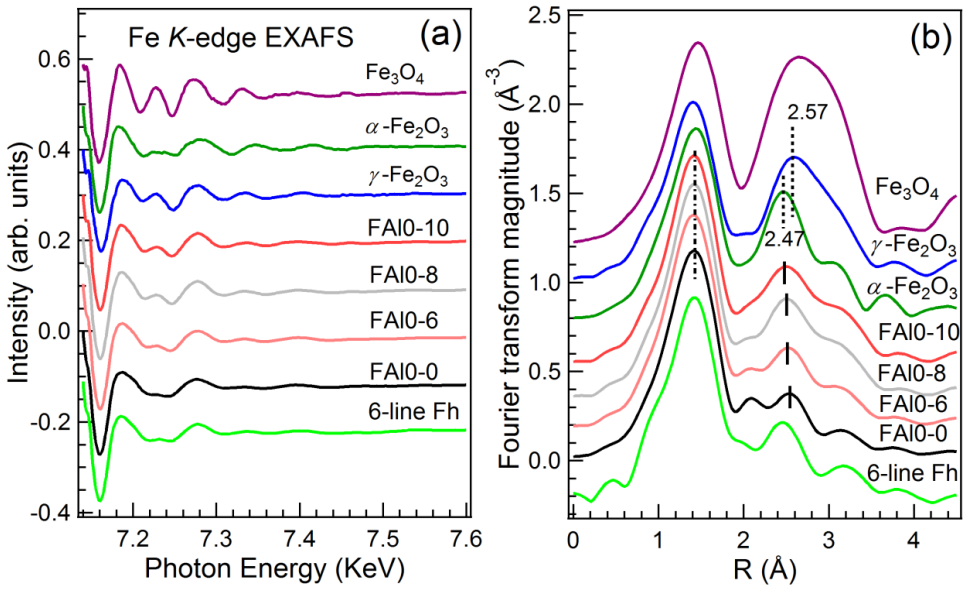

Figure S4. (a) *K*-edge EXAFS spectra for four studied 2-line ferrihydrite samples and standard samples of α-Fe_2O_3, γ-Fe_2O_3, Fe_3O_4 and 6-line ferrihydrite throughout the continuum energy region and (b) corresponding phased-shift uncorrected *K*-edge Fourier transform EXAFS spectra. Fe-Fe associated coordination peaks at ~2.47 Å and ~2.57 Å for α-Fe_2O_3, γ-Fe_2O_3 and Fe_3O_4 are marked by dashed vertical lines, respectively. Solid lines indicate evolution of Fe-Fe coordination peaks for 2-line ferrihydrite with hydrothermal treatment time. The dash-dot line indicates the position of Fe-O coordination peaks for the studied ferrihydrite samples.

The influence of longer-range order on spectra. *L*-edge XAS spectra and *K*-edge XANES spectra for 2-line and 6-line ferrihydrite samples at room temperature are shown in **Figure S5**. XAS spectra at the *L*-edge for two samples were measured using linear polarized soft X-rays. As shown in **Figure S5**, the Fe *L*- and *K*-edge spectra for 2-line ferrihydrite resemble that of 6-line ferrihydrite, although 6-line ferrihydrite has longer-range order than that of 2-line ferrihydrite, which corresponds well with literature reports.[2, 3] It is not surprising that structural disorder has little influence on spectral shape in both *L*-edge XAS and *K*-edge XANES spectra because the spectra are dominated by quasi-atomic transitions, with minor modification from the solid state environment for the *L*-edge,[4] whereas for *K*-edge XANES spectra, the influence of structural order can be largely ignored, as the shape and intensity of main edge features are sensitive to short-range order (particularly the first coordination shell) around sites.

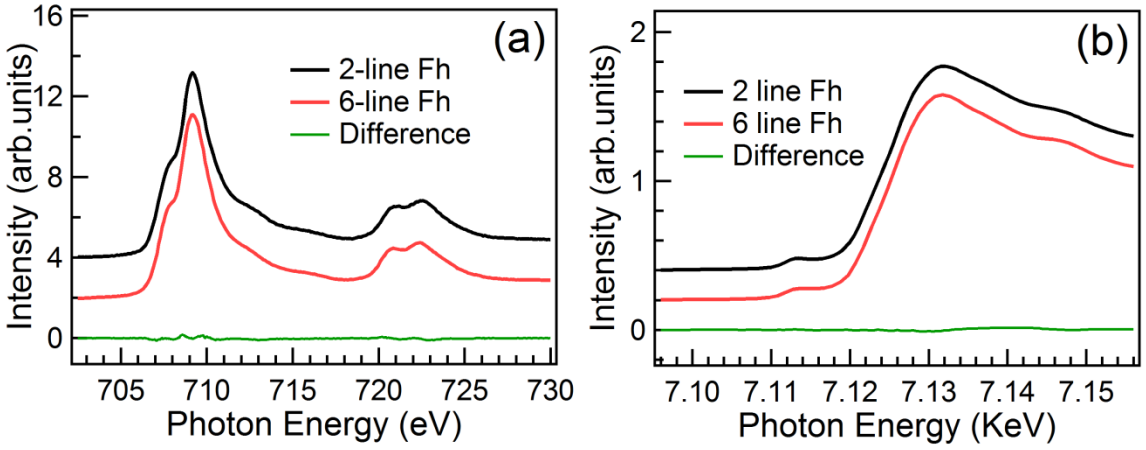

Figure S5. (a) *L*-edge XAS and (b) *K*-edge XANES spectra for 2-line and 6-line ferrihydrite. The difference spectrum is shown at the bottom of each panel.

Oxygen *K*-edge spectra for four studied samples and three reference phases of hematite, maghemite and magnetite are shown in **Figure S6**. The higher energy features between 533 eV and 545 eV are generally attributed to the transition from the O 1*s* to O 2*p* hybridized with the Fe

4*s* and 4*p* states. Pre-edge features in the 528~533 eV region are attributed to the transition from O 1*s* to O 2*p* states hybridized with Fe 3*d* states, which are split into t_{2g} and e_g states due to the oxygen octahedral crystal field.[5,6] The pre-edge features of the magnetite reference have higher positions and slightly worse resolution than that of hematite, which is in accordance with findings reported by *Wu* et al.[7] The formation of goethite is ruled out, otherwise a new feature located at the higher energy side of e_g resonance should emerge,[8,9] which is in good agreement with results from magnetic measurements.[10] It is worth noting that the measured XAS signal has a contribution from oxygen contamination due to air exposure, so that the accuracy of the intensity of each feature is unknown. However, this does not alter the main conclusion that α- and γ- Fe_2O_3 formed and contribute to evolution of the spectral profile at the O *K*-edge for hydrothermally aged ferrihydrite.

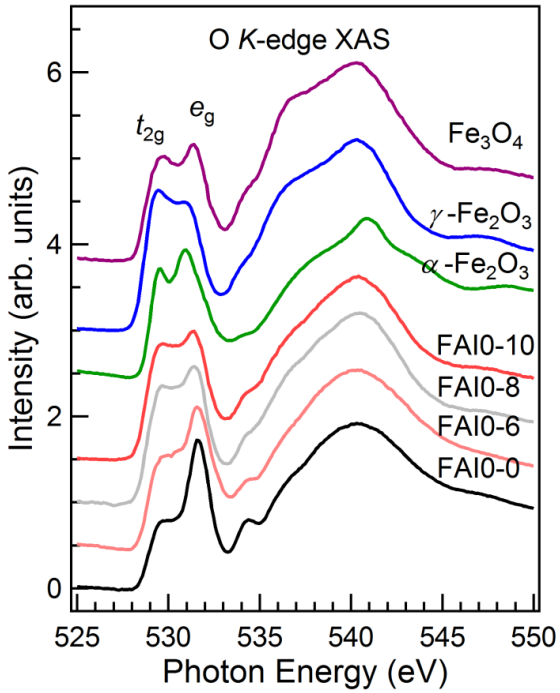

Figure S6. Oxygen *K*-edge XAS spectra for the four studied 2-line ferrihydrite samples and for three reference samples.

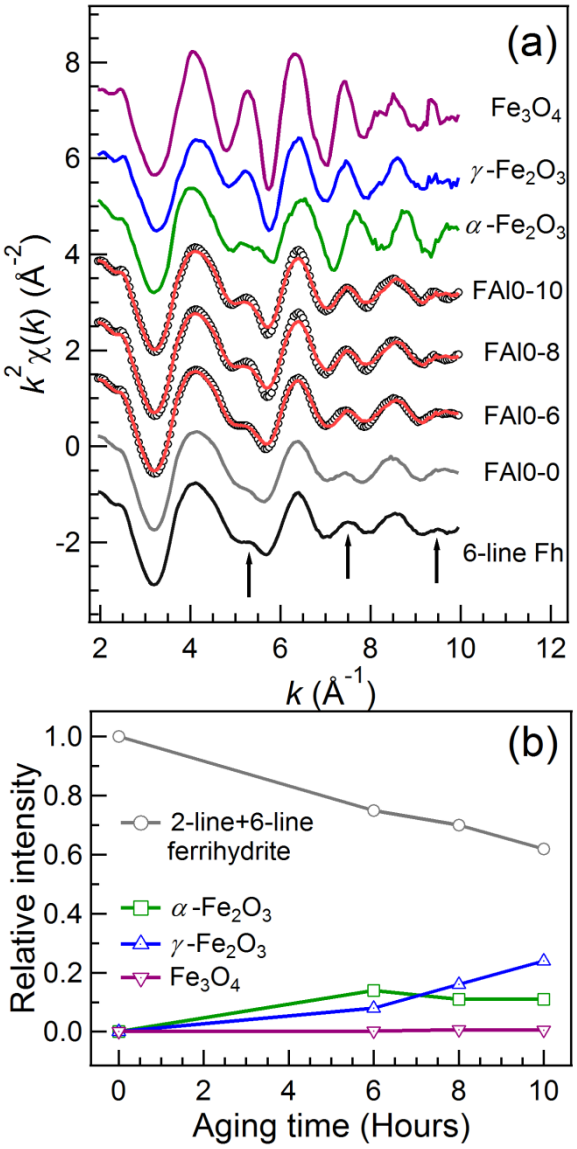

Figure S7. (a) k^2-weighted EXAFS spectra for four studied 2-line ferrihydrite samples, three iron oxide reference samples and a 6-line ferrihydrite reference. Arrows indicate oscillations for ferrihydrite, which are structural order dependent. Red solid lines represent best-fit curves for k = 2-10 Å^{-1}. (b) Concentrations of different Fe oxides as a function of hydrothermal aging time.

In order to validate the linear combination fitting of *K*-edge XANES spectra, linear combination fitting of k spaced EXAFS spectra for studied samples was performed and results are shown as red curves in **Figure S7**(a). Considering the transformation of 6-line ferrihydrite

revealed by XRD and dependence of EXAFS spectra on structural order (arrows in **Figure S7**(a)), a 6-line ferrihydrite reference was selected. Compositions from the best fits are listed in **Table S1**. Evolution of each component vs hydrothermal aging time (**Figure S7**(b)) is consistent with linear combination fitting of *K*-edge XANES spectra, which confirms their validity.

Table S1. Contributions to $k^2\chi(k)$ EXAFS spectra from chemical species present for different hydrothermal aging times.

		$k^2\chi(k)$ EXAFS spectra contribution (%)					
XAS	Sample	FAl0-0	6-line Fh	α-Fe_2O_3	γ-Fe_2O_3	Fe_3O_4	χ^2
K-edge ($k^2\chi(k)$ EXAFS)	FAl0-6	65	10	14	8	3	0.002
	FAl0-8	39	31	11	16	3	0.006
	FAl0-10	35	27	11	25	2	0.005

References

(1) Yang, T.-Y.; Wen, W.; Yin, G.-Z.; Li, X.-L.; Gao, M.; Gu, Y.-L.; Li, L.; Liu, Y.; Lin, H.; Zhang, X.-M.; Zhao, B.; Liu, T.-K.; Yang, Y.-G.; Li, Z.; Zhou, X.-T.; Gao, X.-Y. Introduction of the X-ray diffraction beamline of SSRF. *Nucl. Sci. Tech.* **2015**, 26 (2), 020101.

(2) Masina, C. J.; Neethling, J. H.; Olivier, E. J.; Manzini, S.; Lodya, L.; Srot, V.; van Aken, P. A. Structural and magnetic properties of ferrihydrite nanoparticles. *RSC Adv.* **2015**, *5* (50), 39643-39650.

(3) Carta, D.; Casula, M. F.; Corrias, A.; Falqui, A.; Navarra, G.; Pinna, G. Structural and magnetic characterization of synthetic ferrihydrite nanoparticles. *Mater. Chem. Phys.* **2009**, *113* (1), 349-355.

(4) van der Laan, G.; Kirkman, I. W. The 2*p* absorption spectra of 3*d* transition metal compounds in tetrahedral and octahedral symmetry. *J. Phys.: Condens. Matter* **1992**, *4* (16), 4189.

(5) Signorini, L.; Pasquini, L.; Savini, L.; Carboni, R.; Boscherini, F.; Bonetti, E.; Giglia, A.; Pedio, M.; Mahne, N.; Nannarone, S. Size-dependent oxidation in iron/iron oxide core-shell nanoparticles. *Phys. Rev. B* **2003,** *68* (19), 195423.

(6) Chen, S.-Y.; Gloter, A.; Zobelli, A.; Wang, L.; Chen, C.-H.; Colliex, C. Electron energy loss spectroscopy and *ab initio* investigation of iron oxide nanomaterials grown by a hydrothermal process. *Phys. Rev. B* **2009,** *79* (10), 104103.

(7) Wu, Z. Y.; Gota, S.; Jollet, F.; Pollak, M.; Gautier-Soyer, M.; Natoli, C. R. Characterization of iron oxides by x-ray absorption at the oxygen K edge using a full multiple-scattering approach. *Phys. Rev. B* **1997,** *55* (4), 2570-2577.

(8) Gilbert, B.; Erbs, J. J.; Penn, R. L.; Petkov, V.; Spagnoli, D.; Waychunas, G. A. A disordered nanoparticle model for 6-line ferrihydrite. *Am. Mineral.* **2013,** *98* (8-9), 1465-1476.

(9) Brandt, F.; Schäfer, T.; Claret, F.; Bosbach, D. Heterogeneous formation of ferric oxide nanoparticles on chlorite surfaces studied by x-ray absorption spectromicroscopy (STXM). *Chem. Geol.* **2012,** *329*, 42-52.

(10) Liu, Q.; Barrón, V.; Torrent, J.; Eeckhout, S. G.; Deng, C. Magnetism of intermediate hydromaghemite in the transformation of 2-line ferrihydrite into hematite and its paleoenvironmental implications. *J. Geophys. Res.* **2008,** *113* (B1), B01103.